

Article

# Tensile Properties of Al-12Si Fabricated via Selective Laser Melting (SLM) at Different Temperatures

Konda Gokuldoss Prashanth <sup>1,\*</sup>, Sergio Scudino <sup>2</sup> and Jürgen Eckert <sup>1,3</sup>

<sup>1</sup> Erich Schmid Institute of Materials Science, Austrian Academy of Sciences, Jahnstraße 12, A-8700 Leoben, Austria; juergen.eckert@oeaw.ac.at or juergen.eckert@unileoben.ac.at

<sup>2</sup> Solidification Processes and Complex Structures, Institute for Complex Materials, Leibniz Institute for Solid State and Materials Research (IFW Dresden), Helmholtzstraße 20, D-01069 Dresden, Germany; s.scudino@ifw-dresden.de

<sup>3</sup> Department Materials Physics, Montanuniversität Leoben, Jahnstraße 12, A-8700 Leoben, Austria

\* Correspondence: kgprashanth@gmail.com or Prashanth.kondagokuldoss@oeaw.ac.at; Tel.: +43-3842-804-206; Fax: +43-3482-804-116

Academic Editor: Anders E. W. Jarfors

Received: 13 October 2016; Accepted: 30 November 2016; Published: 2 December 2016

**Abstract:** Additive manufacturing processes such as selective laser melting (SLM) are attracting increasing attention and are regarded as the manufacturing technology of the future, because of their ability to produce near net shaped components of theoretically any shape with added functionality. Various properties, including mechanical, tribological, welding, and corrosion properties, of Al-12Si alloys fabricated via SLM have been extensively studied. However, all of these studies were carried out at ambient conditions. Nevertheless, under working conditions, these alloys experience service temperatures ranging between 373 and 473 K. The present study focuses on the evaluation of the mechanical properties of SLM-fabricated Al-12Si alloys in this temperature range. For this, Al-12Si alloy specimens were annealed at 573 K, a temperature well beyond the test temperature in order to provide a stable microstructure during tensile testing. The plasticity of these materials increases along with the size of the dimples on the fracture surface with increasing tensile test temperature. Moreover, the annealed Al-12Si alloy exhibits appreciable tensile properties when tested between 373 K and 473 K. The results suggest that Al-12Si samples fabricated via SLM may be ideal candidates for automotive applications such as pistons and cylinder heads.

**Keywords:** selective laser melting; light metals; Al-based alloys; mechanical properties

## 1. Introduction

Selective laser melting (SLM), as one of the additive manufacturing processes, is gaining increasing attention from scientists and engineers, because of its ability to produce three-dimensional metallic components of theoretically any shape and with added functionality from three-dimensional computer-aided design data [1–3]. Apart from the ability to produce parts with complex dimensions, the parts generally exhibit very fine microstructures [4,5]. The SLM process involves high cooling rates, which opens up the window of processing even for metallic glasses [6,7]. The SLM process is controlled by several process parameters in order to produce components without defects such as pores or cracks [8–10]. However, most of the work has been focused on selected process parameters that define the energy density, namely, laser power, laser scan speed, layer thickness, spot diameter of the laser, and hatch distance [11,12]. In addition, hatch style also plays a significant role in the SLM fabrication process [13].

A significant amount of SLM research has been devoted to process parameter optimization, which involves a deep understanding of the process and the properties of the employed materials along

with their interaction with the laser [14,15]. Accordingly, several alloy systems have been investigated such as Al-based alloys (mainly Al–Si and Al–Si–Mg) [16–28], where the focus is to develop parts with added functionality and improved properties mainly for automotive and aerospace applications. Fe-based alloys (316L) are developed mainly for structural applications, tooling purposes, and magnetic applications [3,29,30]. Both the biomedical industry and the aerospace industry look to Ti-based alloys as a potential option; there is hence a demand and much research on Ti-based alloy fabrication via SLM [31–35]. Ni-based alloys fabricated via SLM are focused for both high temperature and aerospace applications [36–38]. Processing of Cu-based alloys is not so easy via SLM due to the high conductivity of Cu-based materials. However, some of the Cu-based alloys were fabricated via SLM mainly for parts such as bearings and impellers [39]. CoCr (Mo/W) alloys are another candidate for biomedical applications and can also be used for high temperature applications [40–42]. There are other metals/alloys such as Au/Ag/Pt that have been fabricated via SLM primarily for jewelry industries and some exotic applications [43,44]. The different materials processed via SLM are typically tested at ambient conditions for their mechanical, tribological, or corrosion properties and their bio-medical applicability [16–19,42,45]. Even though these alloy systems have been developed with specific applications in mind, they were not tested under conditions matching the working environment.

Al–Si-based alloys have attracted significant interest because of their low density, wear and corrosion resistance, good castability, machinability, weldability, etc. [46,47]. These properties render Al–Si-based alloys good candidates as engineering components in aerospace and automotive applications [48,49]. However, the service life of the engineering components (e.g., pistons and cylinder heads) depends on several real time factors such as service temperature and environmental conditions. [50–52]. Generally, Al–Si alloys are used when the wear resistance is of utmost interest and the thermal expansion/contraction of the material has to be minimized at the service temperature [53]. Examples include applications for engine components, where the service temperature ranges between 373 and 473 K [54]. However, there have been no reports that deal with the mechanical behavior of Al–Si alloys processed via SLM; hence, it is vital that the behavior of these materials under service temperatures be determined. This forms the basis of the present investigation, where Al-12Si samples fabricated via SLM were tested under uniaxial tension at different temperatures (373, 423, and 473 K). Previous reports have shown that SLM-fabricated Al-12Si exhibits microstructural transformation during heating [18]. Hence, in order to have a stable microstructure and to avoid possible microstructural changes, the SLM-fabricated Al-12Si samples were annealed at 573 K (i.e., well above testing temperatures).

## 2. Materials and Methods

Al-12Si (wt %) gas atomized powder was used to produce bulk samples using SLM processing. A SLM 250 HL device equipped with a Yb-YAG laser (SLM Solutions, Lübeck, Germany) was used for the present study. The samples were built at ambient conditions (stated as room temperature henceforth) using the following parameters: a laser power of 320 W for both contour and volume, a laser scan speed of 1455 mm/s for the volume, and a higher laser speed of 1939 mm/s for the contour. Layers 50  $\mu\text{m}$  thick were used with a hatch spacing of 110  $\mu\text{m}$  and a hatch style rotation of 73° between the layers. The SLM fabrication process was carried out under an argon atmosphere with a slight overpressure inside the building chamber in order to avoid possible oxygen contamination during the process. The oxygen level inside the chamber was kept below 0.2 wt % during the entire building process. Substrate plate heating was not employed during the fabrication process, and the samples were built standing on the substrate plate in the vertical direction. For the present studies, cylindrical tensile bars (according to the standard ASTM: E8/E8M-13a) were built with a total length of 52 mm. The length and diameter of the gauge length were 17.5 mm and 3.5 mm, respectively, and the samples were built on the substrate plate made of the sample material. Support structures were built between the substrate plate and the samples in order to ensure (1) good mechanical stability of the parts, (2) adequate heat dissipation during the building process, and (3) easy removal of the part

from the substrate plate after the fabrication process is complete. The tensile bars were annealed at 573 K for 6 h in an argon atmosphere to avoid oxidation of the samples during the annealing process.

Structural analysis was performed via X-ray diffraction (XRD) using a D3290 PANalytical X'pert PRO (PANalytical, Kassel-Waldau, Germany) X-ray diffractometer in Bragg-Brentano configuration equipped with Co K $\alpha$  ( $\lambda = 0.17889$  nm) radiation along the cross section of the SLM-fabricated samples. Structural refinement of the XRD patterns was carried out by Rietveld profile-fitting using the commercially available software package WinPlotR [55]. The microstructures of the Al-12Si samples before and after the annealing process as well as the surface after tensile tests were examined via scanning electron microscopy (SEM) using a Gemini 1530 microscope (Gemini, Göttingen, Germany) using an accelerating voltage of 10 kV. Tensile tests were carried out at room temperature (300 K) and at 373, 423, and 473 K, severally, using an Instron 8562 (Instron, Darmstadt, Germany) testing facility under quasistatic loading conditions with a strain rate of  $10^{-4}$  s $^{-1}$ . The strain was measured using a conventional extensometer. Three samples were tested under each condition in order to evaluate the repeatability of the test results. The examination of the dimple size was carried out via an image analysis of the corresponding SEM micrographs. Three samples were tested in each case to ascertain the reproducibility, and the most representative curves are shown in the manuscript. Four random lines were superimposed on each micrograph, and three micrographs were used for each sample to estimate the dimple size.

### 3. Results and Discussion

Results for as-prepared SLM-fabricated samples and SLM-fabricated samples annealed at 573 K have been reported elsewhere [18]; only necessary information will be discussed here. The XRD patterns of the as-prepared SLM-fabricated samples and the samples annealed at 573 K are shown in Figure 1. Only the typical diffraction peaks corresponding to the phases Al and Si are observed. The as-prepared SLM-fabricated samples show a unique diffraction pattern, where the intensity of the Al (111) and (200) peaks is reversed, corroborating the presence of texture in the SLM-fabricated material. The Si peaks are not predominant but rather weak in intensity. This suggests a reduced amount of free residual Si (~1 wt %) in the as-prepared material, which is due to the extended solid solubility of Si in Al [17,18]. The lattice parameter of the Al phase is  $0.40508 \pm 0.00002$  nm with crystallite sizes (calculated from the XRD data) of  $118 \pm 2$  nm and  $8 \pm 1$  nm for Al and Si, respectively. With the application of thermal energy, i.e., for the samples annealed at 573 K, the XRD pattern reveals an increase in the intensity of the Al (111) peak at the expense of the (200) peak, suggesting a partial reversal in texture. However, no phase transformation is observed for these samples. On the other hand, the intensity of the Si peaks increases, suggesting that Si is expelled from the supersaturated solid solution of Si in Al. The lattice parameter of Al increases from  $0.40508 \pm 0.00002$  nm in the as-prepared material to  $0.405199 \pm 0.00002$  nm after annealing. This provides direct evidence of Si rejection of the Al matrix. The amount of free residual Si after annealing is ~6 wt % (as compared to ~1 wt % in the as-prepared condition). Simultaneously, the crystallite sizes of Al and Si increase from  $118 \pm 2$  nm and  $8 \pm 1$  nm to  $\sim 120 \pm 2$  nm and  $48 \pm 2$  nm, respectively.

The microstructure of the as-prepared SLM-fabricated samples (Figure 2a,b) shows a typical SLM microstructure, where the laser tracks are visible and the microstructure along the hatch overlaps differs from the core of the tracks. The hatch overlaps involve double melting; hence, the cooling rate is reduced, leading to a coarser microstructure than the track cores. It has also been observed for as-prepared SLM-fabricated Al-12Si samples that the Si concentration is higher along the hatch overlaps [18]. A cellular microstructure is observed in the core of the sample, where the cell boundaries are enriched in Si compared to the cell interior [17,18]. On the other hand, the hatch overlaps show an elongated morphology. The samples annealed at 573 K show a completely different microstructure (Figure 2c,d). With annealing, the rejection of Si from the supersaturated Al phase takes place, and Si precipitates in the form of particles. The Si, which was present along the cell boundaries in the as-prepared sample, diffuses to form particles, and these particles act as nucleation sites for the

precipitation of excess Si from the Al matrix. Hence, the microstructure transforms to a composite-like microstructure consisting of an Al-matrix reinforced with Si particles. The size of the Si particles is  $0.28 \pm 0.01 \mu\text{m}$ , and the Si particle density along the core of the hatches is  $2.69 \pm 0.06 \text{ particles}/\mu\text{m}^2$ . In contrast, the Si particle density along the hatch overlaps ( $6.01 \pm 0.57 \text{ particles}/\mu\text{m}^2$ ) is about twice that of the Si particle density in the core of the hatches.

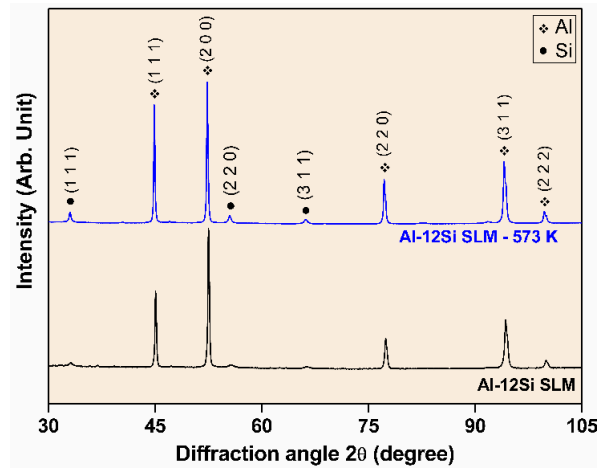


**Figure 1.** X-ray diffraction patterns ( $\lambda = 0.17889 \text{ nm}$ ) for the as-prepared SLM-fabricated Al-12Si samples and samples annealed at 573 K.

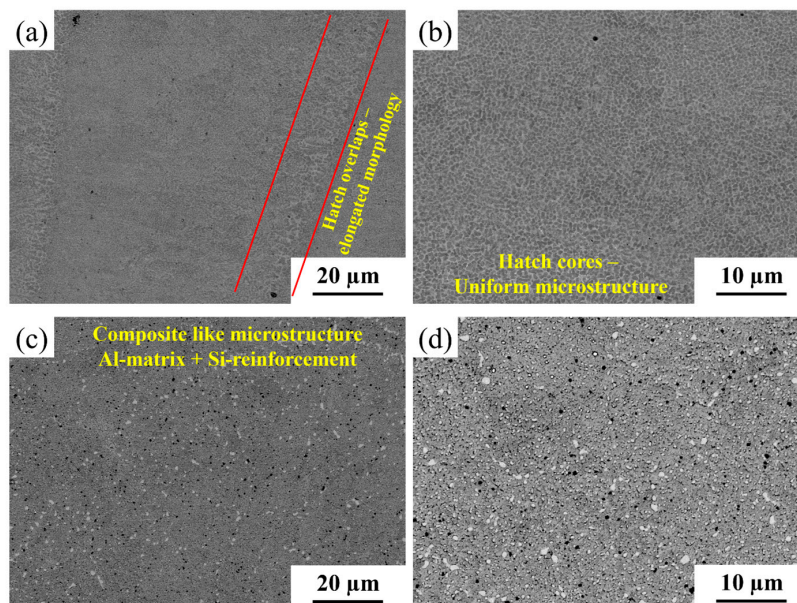


**Figure 2.** Back-scattered scanning electron microscopy images of SLM-fabricated Al-12Si samples along the cross section ( $X$ - $Y$  plane): (a,b) as-prepared; (c,d) annealed at 573 K.

Figure 3a shows the tensile true stress–strain curves of the as-prepared SLM-fabricated samples tested at room temperature and for samples annealed at 573 K at room temperature (300 K), 373, 423, and 473 K, and the corresponding mechanical data are summarized in Figure 3b. The as-prepared SLM-fabricated samples show a yield strength (YS) of  $\sim 240 \pm 1 \text{ MPa}$  and an ultimate tensile strength (UTS) of  $\sim 385 \pm 4 \text{ MPa}$  with  $\sim 3\% \pm 0.1\%$  strain. After annealing the samples at 573 K, the room temperature tensile test results reveal that the YS drops to  $\sim 138 \pm 3 \text{ MPa}$  and the UTS to  $\sim 207 \pm 5 \text{ MPa}$  along with a marginal plasticity improvement to about  $3.8\% \pm 0.2\%$ . The samples annealed at 573 K

were then tested at three different temperatures, i.e., 373, 423, and 473 K. As expected, the material softens when tested at elevated temperatures. The YS decreases from  $138 \pm 3$  to  $114 \pm 4$  MPa and the UTS from  $207 \pm 5$  to  $122 \pm 2$  MPa, when the tensile tests were performed at 300 and 473 K. The softening of the matrix along with grain growth with increasing test temperature leads to less pronounced strain hardening behavior in these samples [51]. However, the plasticity of the samples increases from  $\sim 3.8\% \pm 0.1\%$  to  $5\% \pm 0.3\%$ , suggesting that SLM-fabricated Al-12Si components at their service temperatures lose their strength only marginally, without a drastic change in their fracture strain, which, in turn, shows a marginal improvement. It is interesting to note that the tensile properties at ambient conditions of the specimen annealed at 573 K is similar to those of the Al-12Si samples fabricated via conventional casting [18]; however, the properties observed at 473 K are better than the properties of conventionally cast Al-12Si samples tested at the same temperature [56].

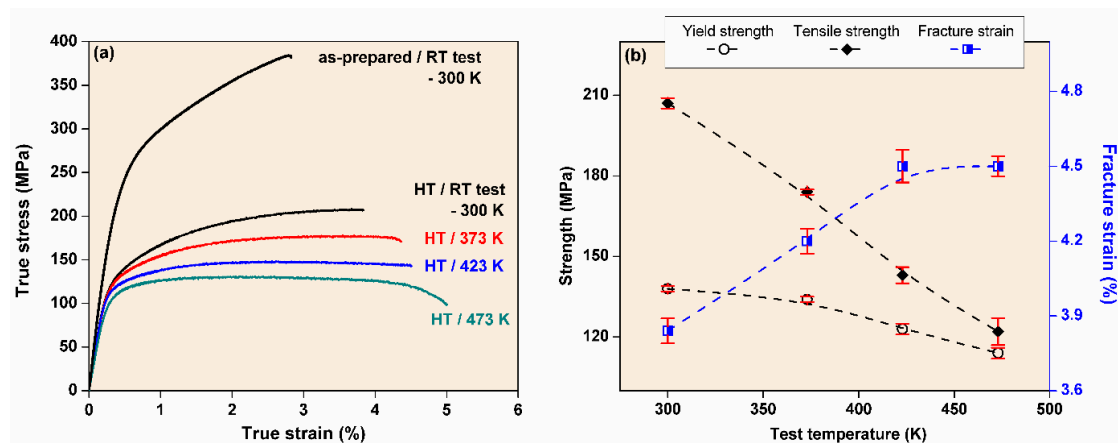


**Figure 3.** (a) Tensile true stress–strain curves for SLM-fabricated Al-12Si samples annealed at 573 K carried out at 300, 373, 423, and 473 K; (b) corresponding mechanical data.

The fracture surfaces of the as-prepared SLM-fabricated samples exhibit submicron-sized dimples, but no Si particles were observed [16,18]. The fracture surfaces of the samples annealed at 573 K (Figure 4a) still show the presence of dimples. However, the size of the dimples is larger than that of the as-prepared SLM-fabricated samples. The fracture morphologies of the samples after the tensile tests were carried out at various temperatures (373, 423, and 473 K) are shown in Figure 4b–d. The size of the Al dimples increases for the samples tested at different temperatures, in agreement with the high-temperature mechanical tests of other Al-based alloys [56]. This increase in dimple size correlates with the softening of the Al matrix at high temperatures, as suggested by the tensile curves in Figure 3. The size of the dimples as a function of tensile test temperature and YS is shown in Figure 5. The size of the dimples increases linearly with increasing test temperature (Figure 5a). Interestingly, a linear correlation is also observed when the YS of the samples is plotted against the dimple size in the form of a Hall–Petch relationship (Figure 5b). The variation of the dimple size is associated with grain coarsening of the matrix, resulting from the additional thermal energy supplied during the tensile test. In order to have a stable microstructure, the Al-12Si samples were annealed at 573 K. However, in reality, the as-prepared samples will be subjected to service without any annealing treatment. Hence, when these components are used as pistons, the service temperature will be initially utilized for the transformation of the microstructure through diffusion and the properties are expected to be better than the properties observed in the present study. Hence, Al-12Si samples fabricated via SLM show promise as highly suitable materials for components in the automobile sector (such as cylinder heads and pistons).

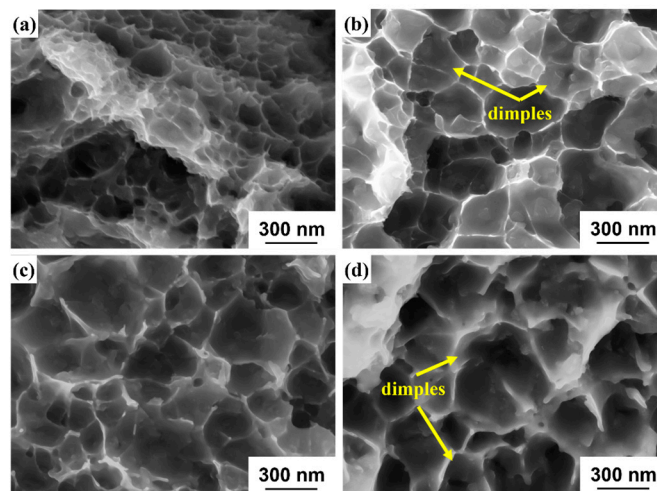


**Figure 4.** Fracture morphology after tensile testing for SLM-fabricated Al-12Si samples annealed at 573 K and deformed at (a) 300 K; (b) 373 K; (c) 423 K; and (d) 473 K.

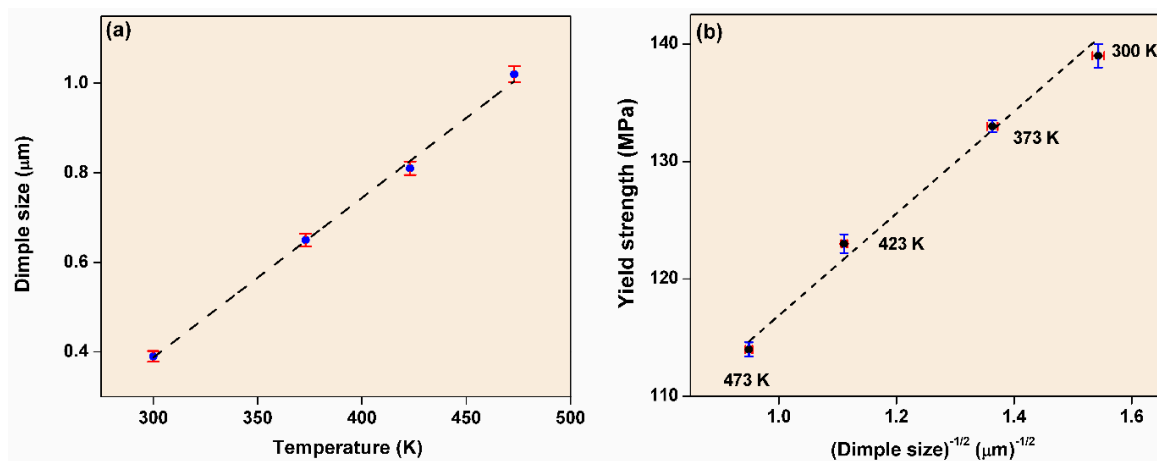


**Figure 5.** (a) Variation of dimple size as a function of the tensile test temperature; (b) yield strength vs. dimple size for the SLM-fabricated Al-12Si samples.

#### 4. Summary

Al-12Si samples produced via SLM have been investigated for their high temperature mechanical properties. The Al-12Si samples were annealed at 573 K in order to obtain a stable microstructure during the tensile tests (which were carried out at 373, 423, and 473 K). The as-prepared supersaturated cellular microstructure transforms to a composite-like microstructure, with the free residual Si particles (~6 wt %) reinforcing the Al matrix. The ultimate tensile strength of the as-prepared Al-12Si samples drops from  $\sim 385 \pm 4$  MPa to  $\sim 207 \pm 5$  MPa after annealing—however, with some marginal improvement in ductility. The samples annealed at 573 K tested at different temperatures (373, 423, and 473 K) show appreciable mechanical properties with a marginal drop in strength, but an appreciable improvement in plasticity at the same time. The plasticity improvement can be directly correlated with the increased size of the dimples (grain coarsening) observed on the fracture surface of these samples. The present study suggests that Al-12Si samples fabricated via SLM are well suited to be utilized as components in the automobile sector such as cylinder heads and pistons.

**Acknowledgments:** The financial support through the German Science Foundation (DFG) under the Leibniz Program (grant EC 111/26-1) and the European Research Council under the ERC Advanced Grant INTELHYB (grant ERC-2013-ADG-340025) is gratefully acknowledged.

**Author Contributions:** K.G.P., S.S., and J.E. conceived and designed the experiments; K.G.P. performed the experiments; K.G.P. and S.S. analyzed the data; K.G.P., S.S., and J.E. contributed to the discussion of the results and the writing of the paper.

**Conflicts of Interest:** The authors declare no conflict of interest.

## References

1. Attar, H.; Löber, L.; Funk, A.; Calin, M.; Zhang, L.C.; Prashanth, K.G.; Scudino, S.; Zhang, Y.S.; Eckert, J. Mechanical behavior of porous commercially pure Ti and Ti-TiB composite materials manufactured by selective laser melting. *Mater. Sci. Eng. A* **2015**, *625*, 350–356. [[CrossRef](#)]
2. Zhuravleva, K.; Bönisch, M.; Prashanth, K.G.; Hempel, U.; Helth, A.; Gemming, T.; Calin, M.; Scudino, S.; Schultz, L.; Eckert, J.; et al. Production of porous  $\beta$ -Type Ti-40Nb alloy for biomedical applications: Comparison of selective laser melting and hot pressing. *Materials* **2013**, *6*, 5700–5712. [[CrossRef](#)]
3. Prashanth, K.G.; Löber, L.; Klauss, H.-J.; Kühn, U.; Eckert, J. Characterization of 316L steel cellular dodecahedron structures produced by selective laser melting. *Technologies* **2016**, *4*, 34. [[CrossRef](#)]
4. Yap, C.Y.; Chua, C.K.; Dong, Z.L.; Liu, Z.H.; Zhang, D.Q.; Loh, L.E.; Sing, S.L. Review of selective laser melting: Materials and applications. *Appl. Phys. Rev.* **2015**, *2*. [[CrossRef](#)]
5. Prashanth, K.G.; Shakur Shahabi, H.; Attar, H.; Srivastava, V.C.; Ellendt, N.; Uhlenwinkel, V.; Eckert, J.; Scudino, S. Production of high strength Al<sub>85</sub>Nd<sub>8</sub>Ni<sub>5</sub>Co<sub>2</sub> alloy by selective laser melting. *Addit. Manuf. Actur.* **2015**, *6*, 1–5. [[CrossRef](#)]
6. Jung, H.Y.; Choi, S.J.; Prashanth, K.G.; Stoica, M.; Scudino, S.; Yi, S.; Kühn, U.; Kim, D.H.; Kim, K.B.; Eckert, J. Fabrication of Fe-based bulk metallic glass by selective laser melting: A parameter study. *Mater. Des.* **2015**, *86*, 703–708. [[CrossRef](#)]
7. Li, X.P.; Kang, C.W.; Huang, H.; Zhang, L.C.; Sercombe, T.B. Selective laser melting of an Al<sub>86</sub>Ni<sub>6</sub>Y<sub>4.5</sub>Co<sub>2</sub>La<sub>1.5</sub> metallic glass: Processing, microstructure evolution and mechanical properties. *Mater. Sci. Eng. A* **2014**, *606*, 370–379. [[CrossRef](#)]
8. Schwab, H.; Prashanth, K.G.; Löber, L.; Kühn, U.; Eckert, J. Selective Laser Melting of Ti-45Nb Alloy. *Metals* **2015**, *5*, 686–694. [[CrossRef](#)]
9. Ma, P.; Jia, Y.D.; Prashanth, K.G.; Scudino, S.; Yu, Z.; Eckert, J. Microstructure and phase formation in Al-20Si-5Fe-3Cu-1Mg synthesized by selective laser melting. *J. Alloys Compd.* **2016**, *657*, 430–435. [[CrossRef](#)]
10. Ma, P.; Prashanth, K.G.; Scudino, S.; Jia, Y.; Wang, H.; Zou, C.; Wei, Z.; Eckert, J. Influence of annealing on mechanical properties of Al-20Si processed by selective laser melting. *Metals* **2014**, *4*, 28–36. [[CrossRef](#)]
11. Dadbakhsh, S.; Hao, L.; Jerrard, P.G.E.; Zhang, D.Z. Experimental investigation on selective laser melting behaviour and processing windows of in situ reacted Al/Fe<sub>2</sub>O<sub>3</sub> powder mixture. *Powder Technol.* **2012**, *231*, 112–121. [[CrossRef](#)]
12. Zhang, H.; Zhu, H.; Qi, T.; Hu, Z.; Zeng, X. Selective laser melting of high strength Al-Cu-Mg alloys: Processing, microstructure and mechanical properties. *Mater. Sci. Eng. A* **2016**, *656*, 47–54. [[CrossRef](#)]
13. Thijs, L.; Kempen, K.; Kruth, J.P.; Van Humbeeck, J. Fine-structured aluminium products with controllable texture by selective laser melting of pre-alloyed AlSi10Mg powder. *Acta Mater.* **2013**, *61*, 1809–1819. [[CrossRef](#)]
14. Yadroitsev, I.; Yadroitsava, I.; Bertrand, P.; Smurov, I. Factor analysis of selective laser melting process parameters and geometrical characteristics of synthesized single tracks. *Rapid Prototyp. J.* **2012**, *18*, 201–208. [[CrossRef](#)]
15. Yilbas, B.S.; Yilbas, Z. Some aspects of laser-metal vapour interaction. *Pramana J. Phys.* **1988**, *31*, 365–381. [[CrossRef](#)]
16. Prashanth, K.G.; Damodaram, R.; Scudino, S.; Wang, Z.; Prasad Rao, K.; Eckert, J. Friction welding of Al-12Si parts produced by selective laser melting. *Mater. Des.* **2014**, *57*, 632–637. [[CrossRef](#)]
17. Prashanth, K.G.; Debalina, B.; Wang, Z.; Gostin, P.F.; Gebert, A.; Calin, M.; Kühn, U.; Kamaraj, M.; Scudino, S.; Eckert, J. Tribological and corrosion properties of Al-12Si produced by selective laser melting. *J. Mater. Res.* **2014**, *29*, 2044–2054. [[CrossRef](#)]

18. Prashanth, K.G.; Scudino, S.; Klauss, H.J.; Surreddi, K.B.; Löber, L.; Wang, Z.; Chaubey, A.K.; Kühn, U.; Eckert, J. Microstructure and mechanical properties of Al-12Si produced by selective laser melting: Effect of heat treatment. *Mater. Sci. Eng. A* **2014**, *590*, 153–160. [[CrossRef](#)]
19. Suryawanshi, J.; Prashanth, K.G.; Scudino, S.; Eckert, J.; Prakash, O.; Ramamurty, U. Simultaneous enhancements of strength and toughness in an Al-12Si alloy synthesized using selective laser melting. *Acta Mater.* **2016**, *115*, 285–294. [[CrossRef](#)]
20. Wang, X.J.; Zhang, L.C.; Fang, M.H.; Sercombe, T.B. The effect of atmosphere on the structure and properties of a selective laser melted Al-12Si alloy. *Mater. Sci. Eng. A* **2014**, *597*, 370–375. [[CrossRef](#)]
21. Aboulkhair, N.T.; Everitt, N.M.; Ashcroft, I.; Tuck, C. Reducing porosity in AlSi10Mg parts processed by selective laser melting. *Addit. Manuf.* **2014**, *1*, 77–86. [[CrossRef](#)]
22. Brandl, E.; Heckenberger, U.; Holzinger, V.; Buchbinder, D. Additive manufactured AlSi10Mg samples using Selective Laser Melting (SLM): Microstructure, high cycle fatigue, and fracture behavior. *Mater. Des.* **2012**, *34*, 159–169. [[CrossRef](#)]
23. Dai, D.; Gu, D. Influence of thermodynamics within molten pool on migration and distribution state of reinforcement during selective laser melting of AlN/AlSi10Mg composites. *Int. J. Mach. Tools Manuf.* **2016**, *100*, 14–24. [[CrossRef](#)]
24. Gu, D.; Wang, H.; Dai, D.; Yuan, P.; Meiners, W.; Poprawe, R. Rapid fabrication of Al-based bulk-form nanocomposites with novel reinforcement and enhanced performance by selective laser melting. *Scr. Mater.* **2015**, *96*, 25–28. [[CrossRef](#)]
25. Prashanth, K.G.; Scudino, S.; Chaubey, A.K.; Löber, L.; Wang, P.; Attar, H.; Schimansky, F.P.; Pyczak, F.; Eckert, J. Processing of Al-12Si-TiN composites by selective laser melting and evaluation of compressive and wear properties. *J. Mater. Res.* **2016**, *31*, 55–65. [[CrossRef](#)]
26. Wang, P.; Li, H.C.; Prashanth, K.G.; Eckert, J.; Scudino, S. Selective laser melting of Al-Zn-Mg-Cu: Heat treatment, microstructure and mechanical properties. *J. Alloys Compd.* **2017**, in press. [[CrossRef](#)]
27. Lam, L.P.; Zhang, D.Q.; Liu, Z.H.; Chua, C.K. Phase analysis and microstructure characterization of AlSi10Mg parts produced by selective laser melting. *Virtual Phys. Prototyp.* **2015**, *10*, 207–215. [[CrossRef](#)]
28. Sing, S.L.; Lam, L.P.; Zhang, D.Q.; Liu, Z.H.; Chua, C.K. Interfacial characterization of SLM parts in multi-material processing: Intermetallic phase formation between AlSi10Mg and C18400 copper alloy. *Mater. Charact.* **2015**, *107*, 220–227. [[CrossRef](#)]
29. Sun, Z.; Tan, X.; Tor, S.B.; Yeong, W.Y. Selective laser melting of stainless steel 316L with low porosity and high build rates. *Mater. Des.* **2016**, *104*, 197–204. [[CrossRef](#)]
30. Wang, D.; Song, C.; Yang, Y.; Bai, Y. Investigation of crystal growth mechanism during selective laser melting and mechanical property characterization of 316L stainless steel parts. *Mater. Des.* **2016**, *100*, 291–299. [[CrossRef](#)]
31. Attar, H.; Prashanth, K.G.; Chaubey, A.K.; Calin, M.; Zhang, L.C.; Scudino, S.; Eckert, J. Comparison of wear properties of commercially pure titanium prepared by selective laser melting and casting processes. *Mater. Lett.* **2015**, *142*, 38–41. [[CrossRef](#)]
32. Attar, H.; Prashanth, K.G.; Zhang, L.C.; Calin, M.; Okulov, I.V.; Scudino, S.; Yang, C.; Eckert, J. Effect of powder particle shape on the properties of in situ Ti-TiB composite materials produced by selective laser melting. *J. Mater. Sci. Technol.* **2015**, *31*, 1001–1005. [[CrossRef](#)]
33. Zhang, L.-C.; Attar, H. Selective laser melting of titanium alloys and titanium matrix composites for biomedical applications: A review. *Adv. Eng. Mater.* **2016**, *18*, 463–475. [[CrossRef](#)]
34. Vandenbroucke, B.; Kruth, J.-P. Selective laser melting of biocompatible metals for rapid manufacturing of medical parts. *Rapid Prototyp. J.* **2007**, *13*, 196–203. [[CrossRef](#)]
35. Vrancken, B.; Thijs, L.; Kruth, J.P.; Van Humbeeck, J. Microstructure and mechanical properties of a novel  $\beta$  titanium metallic composite by selective laser melting. *Acta Mater.* **2014**, *68*, 150–158. [[CrossRef](#)]
36. Amato, K.N.; Gaytan, S.M.; Murr, L.E.; Martinez, E.; Shindo, P.W.; Hernandez, J.; Collins, S.; Medina, F. Microstructures and mechanical behavior of Inconel 718 fabricated by selective laser melting. *Acta Mater.* **2012**, *60*, 2229–2239. [[CrossRef](#)]
37. Lu, Y.; Wu, S.; Gan, Y.; Huang, T.; Yang, C.; Junjie, L.; Lin, J. Study on the microstructure, mechanical property and residual stress of SLM Inconel-718 alloy manufactured by differing island scanning strategy. *Opt. Laser Technol.* **2015**, *75*, 197–206. [[CrossRef](#)]

38. Zhang, B.; Bi, G.; Nai, S.; Sun, C.N.; Wei, J. Microhardness and microstructure evolution of TiB<sub>2</sub> reinforced Inconel 625/TiB<sub>2</sub> composite produced by selective laser melting. *Opt. Laser Technol.* **2016**, *80*, 186–195. [[CrossRef](#)]
39. Scudino, S.; Unterdörfer, C.; Prashanth, K.G.; Attar, H.; Ellendt, N.; Uhlenwinkel, V.; Eckert, J. Additive manufacturing of Cu-10Sn bronze. *Mater. Lett.* **2015**, *156*, 202–204. [[CrossRef](#)]
40. Lu, Y.; Wu, S.; Gan, Y.; Li, Y.; Zhao, C.; Zhuo, C.; Lin, C. Investigation on the microstructure, mechanical property and corrosion behavior of the selective laser melted CoCrW alloy for dental application. *Mater. Sci. Eng. C* **2015**, *49*, 517–525. [[CrossRef](#)] [[PubMed](#)]
41. Zhou, X.; Li, K.; Zhang, D.; Liu, X.; Ma, J.; Liu, W.; Shen, Z. Textures formed in a CoCrMo alloy by selective laser melting. *J. Alloys Compd.* **2015**, *631*, 153–164. [[CrossRef](#)]
42. Hedberg, Y.S.; Qian, B.; Shen, Z.; Virtanen, S.; Odnevall Wallinder, I. In vitro biocompatibility of CoCrMo dental alloys fabricated by selective laser melting. *Dent. Mater.* **2014**, *30*, 525–534. [[CrossRef](#)] [[PubMed](#)]
43. Khan, M.; Dickens, P. Selective laser melting (SLM) of pure gold. *Gold Bull.* **2010**, *43*, 114–121. [[CrossRef](#)]
44. Fateri, M.; Hötter, J.-S.; Gebhardt, A. Experimental and theoretical investigation of buckling deformation of fabricated objects by selective laser melting. *Phys. Procedia* **2012**, *39*, 464–470. [[CrossRef](#)]
45. Li, F.; Li, J.; Kou, H.; Zhou, L. Porous Ti6Al4V alloys with enhanced normalized fatigue strength for biomedical applications. *Mater. Sci. Eng. C* **2016**, *60*, 485–488. [[CrossRef](#)] [[PubMed](#)]
46. Srivastava, V.C.; Mandal, R.K.; Ojha, S.N. Microstructure and mechanical properties of Al-Si alloys produced by spray forming process. *Mater. Sci. Eng. A* **2001**, *304–306*, 555–558. [[CrossRef](#)]
47. Zhou, J.; Duszczyk, J.; Korevaar, B.M. Microstructural features and final mechanical properties of the iron-modified Al-20Si-3Cu-1Mg alloy product processed from atomized powder. *J. Mater. Sci.* **1991**, *26*, 3041–3050. [[CrossRef](#)]
48. Grosselle, F.; Timelli, G.; Bonollo, F. Doe applied to microstructural and mechanical properties of Al-Si-Cu-Mg casting alloys for automotive applications. *Mater. Sci. Eng. A* **2010**, *527*, 3536–3545. [[CrossRef](#)]
49. Kasprzak, W.; Amirkhiz, B.S.; Niewczas, M. Structure and properties of cast Al-Si based alloy with Zr-V-Ti additions and its evaluation of high temperature performance. *J. Alloys Compd.* **2014**, *595*, 67–79. [[CrossRef](#)]
50. Middleton, C.J.; Timmins, R.; Townsend, R.D. The integrity of materials in high temperature components; performance and life assessment. *Int. J. Press. Vessel. Pip.* **1996**, *66*, 33–57. [[CrossRef](#)]
51. Krätschmer, D.; Roos, E.; Schuler, X.; Herter, K.H. Proof of fatigue strength of nuclear components part II: Numerical fatigue analysis for transient stratification loading considering environmental effects. *Int. J. Press. Vessel. Pip.* **2012**, *92*, 1–10. [[CrossRef](#)]
52. Chen, M.; Meng-Burany, X.; Perry, T.A.; Alpas, A.T. Micromechanisms and mechanics of ultra-mild wear in Al-Si alloys. *Acta Mater.* **2008**, *56*, 5605–5616. [[CrossRef](#)]
53. Leatham, A. Spray forming: Alloys, products, and markets. *Met. Powder Rep.* **1999**, *54*, 28–37.
54. Hirsch, J. Automotive trends in aluminium—The European perspective. *Mater. Forum* **2004**, *28*, 15–23.
55. Roisnel, T.; Rodríguez-Carvajal, J. WinPLOTR: A windows tool for powder diffraction pattern analysis. *Mater. Sci. Forum* **2001**, *378–381*, 118–123. [[CrossRef](#)]
56. Choi, S.-H.; Sung, S.-Y.; Choi, H.-J.; Sohn, Y.-H.; Han, B.-S.; Lee, K.-A. High temperature tensile deformation behavior of new heat resistant aluminum alloy. *Procedia Eng.* **2011**, *10*, 159–164. [[CrossRef](#)]

